Composites Part C: Open Access 15 (2024) 100512

Contents lists available at ScienceDirect

Composites Part C: Open Access

journal homepage: www.sciencedirect.com/journal/composites-part-c-open-access

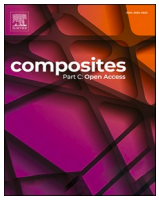

Optimization of functionally graded materials to make stress concentration vanish in a plate with circular hole

Hassan Mohamed Abdelalim Abdalla *, Francesco De Bona, Daniele Casagrande

Polytechnic Department of Engineering and Architecture, University of Udine, Via delle Scienze 206, 33100 Udine, Italy

ARTICLE INFO

Keywords:
Functionally graded materials
Plate with circular hole
Stress concentration factor
Direct transcription
Optimization
Nonlinear programming

ABSTRACT

This paper is devoted to the minimization of the stress concentration factor in infinite plates with circular hole made of functionally graded materials and subjected to a far-field uniform uniaxial tension. Despite the vast literature on the versatility of these materials, the novelty of the results is that the material distribution is not limited to prefixed laws, as in many works available in the literature. Instead, it is assumed to be an unknown piecewise constant function, thus aiming to derive the material distribution by exploiting, at best, the inhomogeneity concept associated with functionally graded materials. After a brief review of the governing equations, the motivation, the statement and the mathematical formulation of the optimization problem are given under the hypothesis of axisymmetric material distribution. Still, the problem could not be solved analytically, therefore a direct transcription approach by the aid of finite difference method has been followed to convert it into a nonlinear programming problem, whose solution has been obtained numerically by dedicated gradient-based solvers. Numerical optimal solutions are reported in graphical forms, thoroughly discussed and validated by means of the finite element method. The developed numerical approach yields a material inhomogeneity obeying a sigmoid-like function and a uniform hoop stress along the radial direction, thus making the stress concentration factor at the rim of the circular hole vanish.

1. Introduction

The study of the stress concentration in panels due to the presence of circular holes constitutes one of the classic problems in mechanics. It is known that if the panel is infinitely large and made of a homogenous, linearly elastic and isotropic material and subjected to a uniform uniaxial tension, then the stress concentration factor (hereinafter abbreviated by SCF) is identically 3. In literature, this result is commonly referred to as the Kirsch solution, named after the German engineer who first described the elastic stresses around the hole [1]. Since then, engineers and researchers have been interested in reducing such a factor by abandoning the aforementioned isotropic and homogeneity assumptions and the shape of the geometrical discontinuity (see, e.g., [2,3] for an exhaustive literature review on various analytical methods).

The adoption of functionally graded materials has propounded its application to numerous mechanical and geotechnical models [4-6], where the microstructure was allowed to vary along one or several directions by employing isotropic, orthotropic or even anisotropic constituent materials (see, e.g., [7-9]). Among all, the stress analysis of functionally graded panels with holes has been investigated. Several analytical and numerical efforts have been carried out aiming at reducing the stress concentration by taking advantage of different inhomogeneity models. For instance, the effect of the material inhomogeneity on the SCF due to circular and elliptic holes are predicted in [10] and [11], respectively, both by means of the finite element method. In particular, Young's modulus has been allowed to vary spatially. Authors have shown that a reduction in the SCF can be obtained by properly choosing the tuning parameters of the heterogeneity factors associated with the property variations (e.g., the exponents in the power- and exponential laws). In [12], the SCF around a circular hole in an infinite plate subjected to uniform biaxial tension and pure shear is analytically solved by exploiting Frobenius series. Closed-form solutions are derived for an exponential variation of Young's modulus along the radius. By dividing the functionally graded plate into a series of piecewise homogeneous radial layers, Refs. [13,14] report the SCFs due to circular holes and under constant loads by means of Muskhelishvili method of the complex variable functions. In [15], closed-form solutions for the SCF at a circular hole in functionally graded panels subject to a

* Corresponding author.
E-mail address: abdalla.hma@spes.uniud.it (H.M.A. Abdalla).

https://doi.org/10.1016/j.jcomc.2024.100512

Available online 18 September 2024

uniform far-field tensile traction are derived by using hypergeometric functions and Frobenius series. Authors show that the SCF at the circular hole can be considerably reduced by appropriately grading the mechanical properties along the radial direction. The elastic response of a functionally graded annular ring inserted in a hole of a homogeneous plate is derived analytically in [16,17] under different far-field loading conditions. All the aforementioned works report a considerable stress concentration reduction only when the Young's modulus progressively increases away from the hole. Moreover, it is observed that the variation of the Poisson's ratio on the stress distribution in the plate is negligible [15-17].

The aforementioned considerations bring into mind the possibility of exploiting optimization theory to enhance the elastic performance of such structures. Many solutions have been proposed to different problems [18,19], some of which are capable of handling only one-dimensional material distribution with one-dimensional geometry and simple loads, while others can tackle more sophisticated problems. Interesting results in terms of stress reduction have been achieved when considering models such as beams, cylindrical shells, rotating disks, pressure vessels and plates (see, e.g., [20-34]), however by imposing prefixed laws for the variation of mechanical properties. In this way, the optimization problems reduce to the search for the heterogeneity factors associated with functional models describing these property variations. On the other hand, other works dealt with the search for the best material distribution to enhance the elastic stress performance *without* prefixing the functional model. Some of these are developed within an analytical tailoring framework [35,36], whereas others rely on phase-field and topology optimization [37,38] or exploit principles from the optimal control theory [39-41]. As far as infinite plates with a circular hole are concerned, the overwhelming research works impose the Young's modulus a priori to forecast the stress concentration near the hole. In the uniaxial load case, to the extent of the authors' knowledge, Ref. [42] is the only work where the unknown Young's modulus distribution is sought in plates with different holes and cutouts, in which enhanced stress results have been obtained by developing an evolutionary algorithm combined with the finite element method. It is worth noting that the iteration process for updating the Young's modulus in each element was governed by a power-law function of local and global stress measures. The stiffness was thus reduced only in the elements whose stresses were higher than an imposed threshold. Although this rule-of-thumb stiffness modification led to enhanced SCFs, we strongly believe that optimal solutions can be achieved if the stiffness optimization is carried out in a more global sense. Accordingly, the objective of the present article is to seek the Young's modulus distribution around the circular hole such that the hoop stress reaches its minimum value along prescribed directions.

The article is organized as follows. Section 2 recalls the governing equations for the plane stresses in linearly elastic, isotropic and inhomogeneous plates. Section 3 aims at presenting the motivation of the work as well as the formulation of the optimization problem. Section 4 illustrates the direct transcription approach as a numerical procedure to convert the optimization problem into a nonlinear programming problem, whose solution has been computed by resorting to a solver available in the literature. The optimal solution of a study case, its validation by a finite element model and its discussion are shown in Section 5 and conclusions are drawn in Section 6.

2. Governing equations

Consider a linearly elastic, isotropic and functionally graded infinite plate with a circular hole of radius a. Let the thickness of the plate be sufficiently small to the point that the stress state is two-dimensional (plane-stress condition). Let the plate be subject to a far-field uniaxial traction σ_0, as shown in Fig. 1a, where the generic point P is described by the polar coordinate system (r, θ), whose origin is at the center of the circular hole, and MN denotes the vertical line associated with the polar angle $\theta = \pi/2$. Moreover, let the inhomogeneity be described by the radial variation of the volume fraction $V(r)$ of one of the two constituents of the functionally graded material (e.g. material #2), which in turn are linked to the effective Young's modulus $E(r)$ by the well-known Voigt estimate

$$E(r) = \widetilde{E}_1(1 - V(r)) + \widetilde{E}_2 V(r), \tag{1}$$

where $\widetilde{E}_1$ and $\widetilde{E}_2$ denote the Young's moduli of the constituents (e.g., metallic and ceramic materials), while the Poisson's ratio ν is assumed to be constant and not affected by the volume fraction. It is worthwhile to note Eq. (1) is adopted in this study since it can be considered as the simplest homogenization technique among the several approaches in micromechanics [43].

2.1. Equilibrium, constitutive and compatibility equations

Next, equations describing the mechanical behavior of the plate are listed. In the absence of body forces, the equilibrium equations read [44]

$$\frac{\partial \sigma_r(r,\theta)}{\partial r} + \frac{1}{r}\frac{\partial \sigma_{r\theta}(r,\theta)}{\partial \theta} + \frac{\sigma_r(r,\theta) - \sigma_\theta(r,\theta)}{r} = 0, \tag{2a,b}$$

$$\frac{\partial \sigma_{r\theta}(r,\theta)}{\partial r} + \frac{1}{r}\frac{\partial \sigma_\theta(r,\theta)}{\partial \theta} + \frac{2}{r}\sigma_{r\theta}(r,\theta) = 0,$$

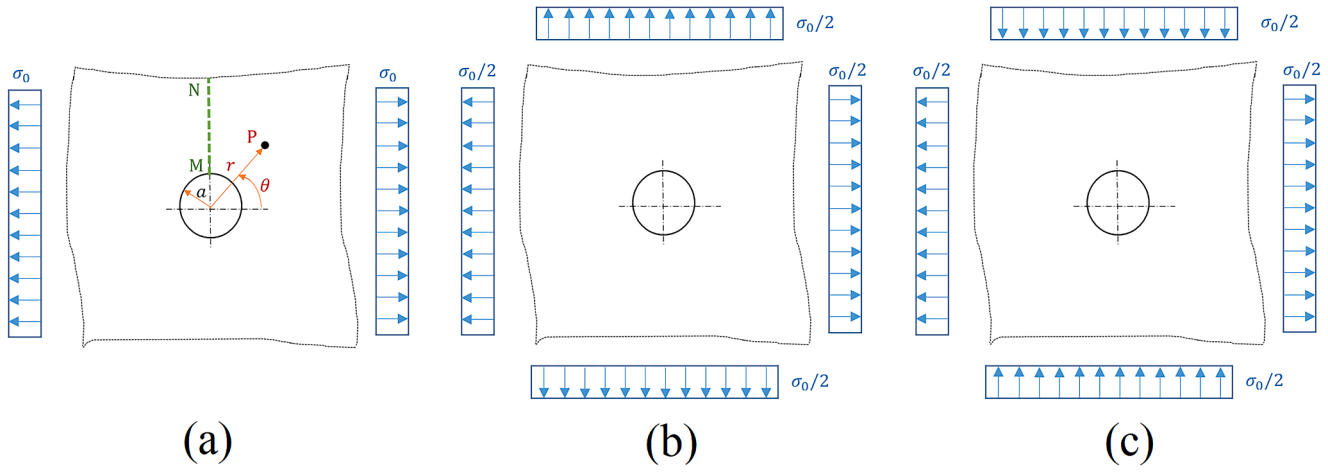

Fig. 1. A schematic representation of (a) an infinite plate with a circular hole subject to a far-field uniaxial traction and its split into (b) uniform biaxial and (c) pure shear sub-problems.

where σ_r, σ_θ and $\sigma_{r\theta}$ are the radial, hoop and shear stresses, respectively, all functions of the radial r and circumferential θ coordinates. The elastic stresses are related to the corresponding strains by the plane-stress constitutive equations, namely [44]

$$E(r)\ \varepsilon_r(r,\theta) = \sigma_r(r,\theta) - \nu\ \sigma_\theta(r,\theta), \tag{3a-c}$$

$$E(r)\ \varepsilon_\theta(r,\theta) = \sigma_\theta(r,\theta) - \nu\ \sigma_r(r,\theta),$$

$$E(r)\ \varepsilon_{r\theta}(r,\theta) = 2(1+\nu)\ \sigma_{r\theta}(r,\theta),$$

where ε_r, ε_θ and $\varepsilon_{r\theta}$ are the radial, hoop and shear strains, respectively, which obey the following compatibility equation [44]

$$\frac{\partial^2\varepsilon_\theta}{\partial r^2} + \frac{1}{r^2}\frac{\partial^2\varepsilon_r}{\partial\theta^2} + \frac{2}{r}\frac{\partial\varepsilon_\theta}{\partial r} - \frac{1}{r}\frac{\partial\varepsilon_r}{\partial r} = \frac{1}{r}\frac{\partial^2\varepsilon_{r\theta}}{\partial r\partial\theta} + \frac{1}{r^2}\frac{\partial\varepsilon_{r\theta}}{\partial\theta}\ . \tag{4}$$

2.2. Superposition of stresses

Due to the linearity hypothesis, if the elastic problem is split into two sub-problems, namely the biaxial problem and the pure shear problem (Figs. 1b,c, respectively, see [44]), the superposition of their solutions leads to the solution of the original one. In other words, letting superscripts "*bx*" and "*ps*" denote respectively the uniform biaxial and pure shear terms, stresses can be written as

$$\sigma_r(r,\theta) = \sigma_r^{bx}(r) + \sigma_r^{ps}(r,\theta), \tag{5a-c}$$

$$\sigma_\theta(r,\theta) = \sigma_\theta^{bx}(r) + \sigma_\theta^{ps}(r,\theta),$$

$$\sigma_{r\theta}(r,\theta) = \sigma_{r\theta}^{ps}(r,\theta),$$

where it is emphasized that stresses for the biaxial problem depend on the radial coordinate only, since the geometry of the problem, the assumed nature of the inhomogeneity and the far-field loading are axisymmetric (and therefore $\sigma_{r\theta}^{bx}$ is identically zero). Substitution of the constitutive relations Eqs. (3a-c) into the compatibility Eq. (4) yields the following boundary-value problem for the radial stress

$$\mathscr{B}\mathscr{X}\left(\sigma_r^{bx}(r)\right) = 0, \qquad a \le r < \infty \tag{6a-c}$$

$$\sigma_r^{bx}(a) = 0,$$

$$\lim_{r\to\infty}\sigma_r^{bx}(r) = \frac{\sigma_0}{2},$$

where the differential operator $\mathscr{B}\mathscr{X}(\cdot)$ is given by $\frac{d^2(\cdot)}{dr^2} + \alpha^{bx}(r)\frac{d(\cdot)}{dr} + \beta^{bx}(r)\ (\cdot)$ with $\alpha^{bx} = \frac{3}{r} - \frac{1}{E}\frac{dE}{dr}$ and $\beta^{bx} = (\nu-1)\frac{1}{rE}\frac{dE}{dr}$.

Moreover, the hoop stress can be obtained from the equilibrium Eq. (2a)

$$\sigma_\theta^{bx}(r) = \sigma_r^{bx}(r) + r\frac{d\sigma_r^{bx}(r)}{dr}\ . \tag{7}$$

In parallel, and similar to the Kirsch solution, the pure shear problem can be solved by introducing the Airy stress function $\varphi(r,\theta)$ as follows [44]

$$\sigma_r^{ps}(r,\theta) = \frac{1}{r}\frac{\partial\varphi(r,\theta)}{\partial r} + \frac{1}{r^2}\frac{\partial^2\varphi(r,\theta)}{\partial\theta^2}, \tag{8a-c}$$

$$\sigma_\theta^{ps}(r,\theta) = \frac{\partial^2\varphi(r,\theta)}{\partial r^2},$$

$$\sigma_{r\theta}^{ps}(r,\theta) = -\frac{\partial}{\partial r}\left(\frac{1}{r}\frac{\partial\varphi(r,\theta)}{\partial\theta}\right),$$

where φ has the form [44]

$$\varphi(r,\theta) = g(r)\cos 2\theta. \tag{9}$$

Consequently, Eqs. (8a-c) read

$$\sigma_r^{ps}(r,\theta) = \left(\frac{1}{r}\frac{dg(r)}{dr} - \frac{4g(r)}{r^2}\right)\cos 2\theta, \tag{10a-c}$$

$$\sigma_\theta^{ps}(r,\theta) = \frac{d^2g(r)}{dr^2}\cos 2\theta,$$

$$\sigma_{r\theta}^{ps}(r,\theta) = 2\left(\frac{1}{r}\frac{dg(r)}{dr} - \frac{g(r)}{r^2}\right)\sin 2\theta.$$

Combining Eqs. 10a-c and 3a-c, the compatibility Eq. (4) reduces to the following differential equation

$$\mathscr{P}\mathscr{S}(g(r)) = 0, \qquad a \le r < \infty \tag{11}$$

where the differential operator $\mathscr{P}\mathscr{S}(\cdot)$ is given by $\frac{d^4(\cdot)}{dr^4} + \alpha^{ps}(r)\frac{d^3(\cdot)}{dr^3} + \beta^{ps}(r)\frac{d^2(\cdot)}{dr^2} + \gamma^{ps}(r)\frac{d(\cdot)}{dr} + \delta^{ps}(r)(\cdot)$ with $\alpha^{ps} = \frac{2}{r} - \frac{2}{E}\frac{dE}{dr}$, $\beta^{ps} = -\frac{1}{E}\frac{d^2E}{dr^2} + \frac{2}{E^2}\left(\frac{dE}{dr}\right)^2 + \frac{\nu}{rE}\frac{dE}{dr} - \frac{2}{rE}\frac{dE}{dr} - \frac{9}{r^2}$, $\gamma^{ps} = \frac{\nu}{rE}\frac{d^2E}{dr^2} - \frac{2\nu}{rE^2}\left(\frac{dE}{dr}\right)^2 + \frac{9}{r^2E}\frac{dE}{dr} + \frac{9}{r^3}$ and $\delta^{ps} = -\frac{4\nu}{r^2E}\frac{d^2E}{dr^2} + \frac{8\nu}{r^2E^2}\left(\frac{dE}{dr}\right)^2 - \frac{12}{r^3E}\frac{dE}{dr}$.

Relation Eq. (11) is a fourth-order linear differential equation with variable coefficients, and it is solved by considering the following boundary conditions

$$\sigma_r^{ps}(a,\theta) = 0, \tag{12a-d}$$

$$\sigma_{r\theta}^{ps}(a,\theta) = 0,$$

$$\lim_{r\to\infty}\sigma_r^{ps}(r,\theta) = \frac{\sigma_0}{2}\cos 2\theta,$$

$$\lim_{r\to\infty}\sigma_{r\theta}^{ps}(r,\theta) = -\frac{\sigma_0}{2}\sin 2\theta\ .$$

The set of the above equations for the two sub-problems can be found in [15].

3. The optimization problem: motivation and formulation

Stresses for the case of a homogeneous infinite plate with a circular hole and subject to a uniaxial traction can be determined by taking Young's modulus as constant in the aforementioned equations, leading to the well-known Kirsch stress field [44]

$$\sigma_r(r,\theta) = \frac{\sigma_0}{2}\left(1 - \frac{a^2}{r^2}\right) + \frac{\sigma_0}{2}\left(1 + \frac{3a^4}{r^4} - \frac{4a^2}{r^2}\right)\cos 2\theta, \tag{13a-c}$$

$$\sigma_\theta(r,\theta) = \frac{\sigma_0}{2}\left(1 + \frac{a^2}{r^2}\right) - \frac{\sigma_0}{2}\left(1 + \frac{3a^4}{r^4}\right)\cos 2\theta,$$

$$\sigma_{r\theta}(r,\theta) = -\frac{\sigma_0}{2}\left(1 - \frac{3a^4}{r^4} + \frac{2a^2}{r^2}\right)\sin 2\theta.$$

It can be easily shown that the SCF at the rim of the circular hole is identically 3 by taking the limit of Eq. (13b) for $r \to a$ and $\theta = \pi/2$ and dividing by σ_0. This value has been drastically reduced by replacing homogeneous materials by functionally graded ones. For instance, according to [15], one can reduce the SCF at the rim of the hole by suitably varying the two heterogeneity factors n and β, linked to the Young's modulus through the relation

$$E(r) = E_\infty\left[1 + \beta\left(\frac{r}{a}\right)^n\right], \tag{14}$$

where $E_\infty = \lim_{r\to\infty}E(r)$, $-1 < \beta < 1$ and $n < 0$ (Fig. 2a shows the radial

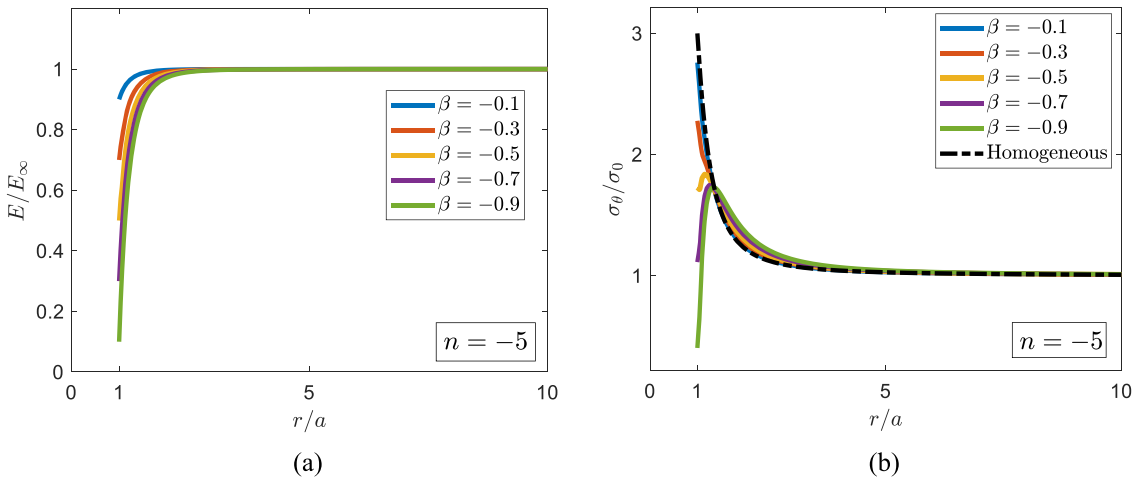

Fig. 2. (a) Variation of Young's modulus with r/a for $n = -5$ and for different values of $\beta < 0$. (b) The associated hoop stresses (solid lines) alongside with Kirsch solution (dashed line) on the vertical line MN. Stresses associated with other Young's modulus distributions are addressed in [15].

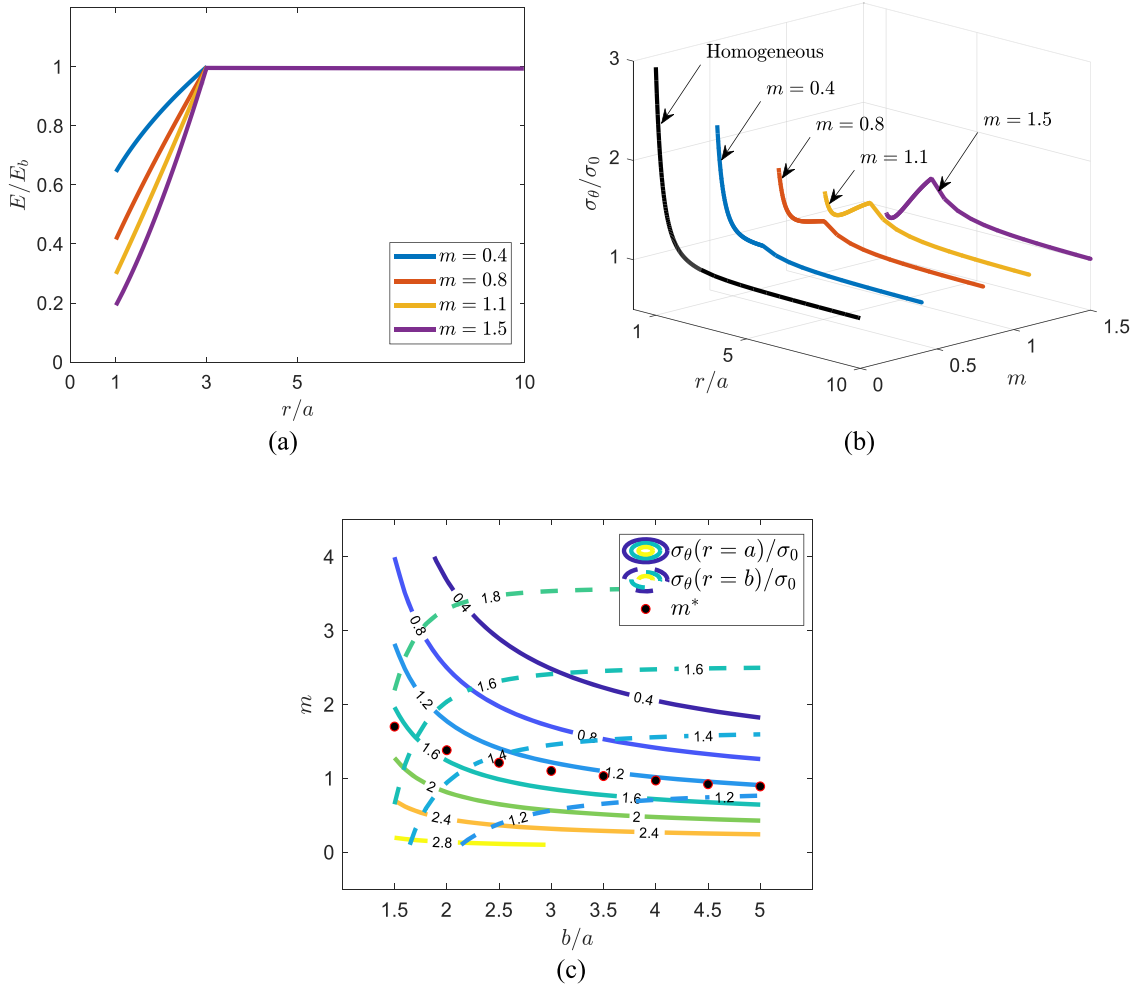

Fig. 3. (a) Variation of Young's modulus with $b/a = 3$ and for different values of $m > 0$. (b) The associated hoop stresses on the vertical line MN alongside with the Kirsch solution. (c) Contour levels for SCFs at the rim of the circular hole (solid contours), the interface between the ring and the homogeneous media (dashed contours) and best homogeneous factors m^* (scatter points). Stresses associated with other ring radii are addressed in [16].

distribution of Young's modulus for $n = -5$ and for different instances of $\beta < 0$). A similar relation for Poisson's ratio has been employed with different heterogeneity factors, but it was found that it does not affect stresses significantly (for this problem, the order of discrepancy is <1 %). Expressions for the associated stress field on MN are lengthy and therefore omitted in this article, but represented in a graphical form in Fig. 2b (see [15]). It is important to notice that although the SCF may arbitrarily tend to 0^+, an increase of the hoop stress occurs elsewhere along the radius, say at $r = \widetilde{a}$. Denoting here after by $\widehat{\sigma}_\theta(r)$ the hoop stress along the vertical line MN, such inevitable increase takes place due to the equilibrium between the applied load and forces resulting from occurring hoop stresses along the line associated with $\theta = \pi/2$.

Thus, the optimum scenario, for the Young's modulus distribution (14), occurs when the heterogeneity factors lead to a constant hoop stress for $r \in [a, \widetilde{a}]$, or, *lato sensu*, to a hoop stress whose standard deviation (or statistical variation) is as minimum as possible. This problem has not been addressed in [15], as authors focused on finding analytical solutions for stresses. The formulation of the SCF minimization problem without remarkably increasing the hoop stress along the radius has been addressed in [16], albeit for a homogeneous isotropic infinite plate endowed with a functionally graded ring of radius $b > a$, where the Young's modulus distribution is given by

$$E(r) = E_b\left(\frac{r}{b}\right)^m, \tag{15}$$

where E_b is the Young's modulus at $r = b$ and m is a real positive number playing the role of the heterogeneity factor (see Fig. 3a where different Young's modulus distributions are shown).

Also here, Poisson's ratio ν is assumed constant and equal to the value of the homogeneous medium. Unlike [15], however, the author not only discussed the analytical tractability of the stress field (whose expression is omitted in this article), but also gave hints on the choice of the best heterogeneity factor for the optimum distribution for the hoop stress throughout the plate. In other words, the author showed that, regardless of the ring geometry, there exists a value of m, say m^*, such that the hoop stress assumes the same value at $r = a$ and $r = b$and less elsewhere, provided that the search for m^* takes place in the range [16]

$$0 < m^* \leq \frac{8(2-\sqrt{3})}{\nu - 7 + 4\sqrt{3}} \tag{16}$$

to avoid complex values for the stress field. Fig. 3b shows the normalized hoop stresses along the vertical line MN for different instances of m and for $b/a = 3$ and compared with Eq. (13b). It is shown that the value of the best heterogeneity factor is approximately $m^* = 1.1$ [16]. For completeness, it is desired to study the dependence of m^* on the geometry of the ring. A possible way is to compute contour levels for the SCFs at the rim of the circular hole and at the interface of the ring with the homogeneous medium for a range of admissible m, in the sense of the upper and lower limits given by Eq. (16), and for different values of b/a. By construction, the intersection of the two contour levels thus helps the reader identify the best heterogeneity factors m^* for fixed values of the ring geometry b/a. This practical chart is shown in Fig. 3c, where the values for m^* are represented by scatter points. It is worth noting that the optimum heterogeneity factor monotonically decreases as b/a increases, namely a stiffer material at the circular hole is needed to compensate for the increase in the ring radius.

Based on the aforementioned considerations, an optimization problem in which the distribution of Young's modulus is sought for the minimization of the SCF arises. In order to avoid stress peaks along the radial direction the goal of minimizing the SCF can be replaced by the minimization of the maximum hoop stress along the line MN (see Fig. 1a), namely

$$\widehat{\sigma}_{\theta,\max} = \max_{r \geq a} \widehat{\sigma}_\theta(r), \tag{17}$$

as the hoop stress, for any (axisymmetric) Young's modulus variation, is expected to reach its peak only along this line. Hence, the optimization problem consists in finding the Young's modulus distribution (or, through Eq. (1), the volume fraction) along the radial direction such that the maximum value for the hoop stress along MN reaches its minimum value, namely

Problem 1.	min $V(r)$	Eq. (17),
	s.t.	(Eq. (1)), Eqs. (5a-c), Eqs. (6a-c), Eq. (11), Eqs. (12a-d) .

Consequently, Problem 1 does not assume any a priori functional form of Young's modulus along the radial direction. The derivation of Problem 1 is sketched in the left part of the flowchart reported in Fig. 4. In the same figure, also the discretizing technique and the optimization solver, described in detail in Section 4, are represented.

In the parlance of optimization theory, Problem 1 is referred to as *dynamic* optimization problem, namely an optimization problem whose decision variables are unknown piecewise continuous functions living in a certain domain, and constraints are differential relations. Solution to Problem 1 is cumbersome from the analytical viewpoint, requiring one to resort to numerical methods. Among all, the so-called direct transcription approach is used, which helps convert the dynamic optimization problem into a nonlinear programming (NLP) problem, namely to an optimization problem whose decision variables are collected in a finite-dimensional vector and constraints consist in equality or inequality algebraic relations. The conversion of algebraic and differential constraints Eqs. (5a-c)-(6a-c) and (11)-(12a-d) into algebraic ones can be carried out by classic numerical methods in mechanics such as the finite element, finite volume, or finite difference methods. In this article, the latter method is employed because the governing equations for stresses Eqs. (6a-c) and (12a-d) were revealed to be functions of the radial coordinate only (and therefore 1D), not to mention the simplicity of the geometrical domain and the prescription of boundary conditions of the problem under consideration. The use of finite element method, instead, would require the adoption of plane elements, which are naturally 2D, unless *ad-hoc* 1D finite elements are developed along the line MN. Hence, the governing equations for the biaxial and pure shear problems are solved by the finite difference method, which is recalled in the next Section for the sake of a self-contained work. Subsequently, to validate the finite difference code, an infinite functionally graded plate with a prefixed Young's modulus distribution of the form (14) is numerically solved and compared to analytical solutions in [15].

4. Direct transcription approach

Hereinafter, the discretization scheme and matrices assembly are performed along the vertical line MN (i.e., with $\theta = \pi/2$) up to a limit radius A sufficiently large (namely $a \ll A < \infty$). Denoting by K the number of (equally distant) discretization points r_k ($k = 1, 2, \ldots, K$) and letting $r_1 = a$ and $r_k = A$, Table 1 lists the finite difference expressions employed to substitute the different derivatives appearing in the governing equations at the generic node r_k, where Ψ generically represents the unknown variable, i.e., either σ_r^{bx} in Eq. (6a) or g in Eq. (11), and $\Delta r = \frac{A-a}{K-1}$ denotes the radial step. Finite difference approximation terms have been chosen to guarantee a second-order accuracy.

Firstly, the finite difference method is applied to Eqs. (6a-c). Taking into account the different expressions in Table 1, and after some algebra, Eq. (6a) can be rewritten as the following system of $K-2$ algebraic equations

$$\sigma_{r\,k+1}^{bx}\left(2 + \Delta r\, \alpha_k^{bx}\right) + \sigma_{r\,k}^{bx}\left(-4 + 2\Delta r^2\, \beta_k^{bx}\right) + \sigma_{r\,k-1}^{bx}\left(2 - \Delta r\, \alpha_k^{bx}\right) = 0, \tag{18}$$

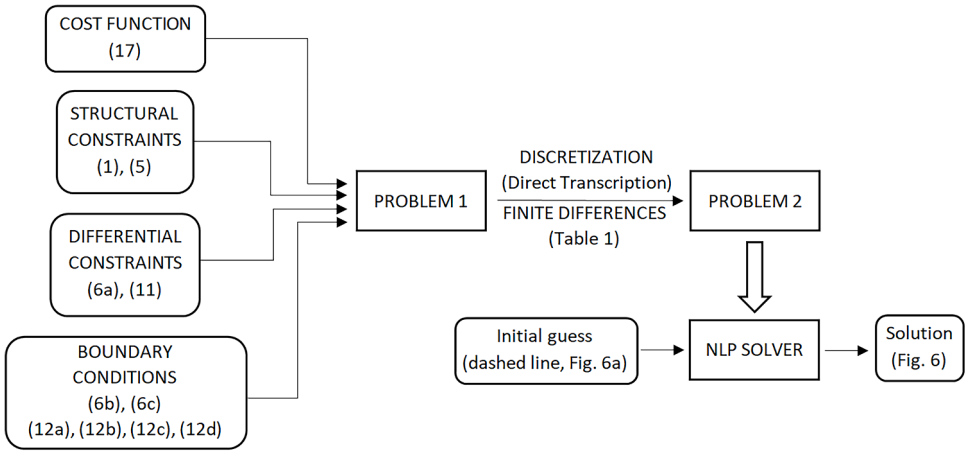

Fig. 4. Flowchart of the employed method.

Table 1
Second-order accuracy expressions for the finite difference terms for the approximation of the different derivatives [45]. Here, Ψ_k denotes the value of Ψ at the generic node r_k.

Node	Derivative	Approximation
First	Forward 1st derivative	$\frac{d\Psi}{dr} \approx \frac{-\Psi_3 + 4\Psi_2 - 3\Psi_1}{2\Delta r}$
	Forward 2nd derivative	$\frac{d^2\Psi}{dr^2} \approx \frac{2\Psi_1 - 5\Psi_2 + 4\Psi_3 - \Psi_4}{\Delta r^2}$
Last	Backward 1st derivative	$\frac{d\Psi}{dr} \approx \frac{\Psi_{K-2} - 4\Psi_{K-1} + 3\Psi_K}{2\Delta r}$
	Backward 2nd derivative	$\frac{d^2\Psi}{dr^2} \approx \frac{-\Psi_{K-3} + 4\Psi_{K-2} - 5\Psi_{K-1} + 2\Psi_K}{\Delta r^2}$
Intermediate	Central 1st derivative	$\frac{d\Psi}{dr} \approx \frac{\Psi_{k+1} - \Psi_{k-1}}{2\Delta r}$
	Central 2nd derivative	$\frac{d^2\Psi}{dr^2} \approx \frac{\Psi_{k+1} - 2\Psi_k + \Psi_{k-1}}{\Delta r^2}$
	Central 3rd derivative	$\frac{d^3\Psi}{dr^3} \approx \frac{\Psi_{k+2} - 2\Psi_{k+1} + 2\Psi_{k-1} - \Psi_{k-2}}{2\Delta r^3}$
	Central 4th derivative	$\frac{d^4\Psi}{dr^4} \approx \frac{\Psi_{k+2} - 4\Psi_{k+1} + 6\Psi_k - 4\Psi_{k-1} + \Psi_{k-2}}{\Delta r^4}$

with k=2,3,…,K−1,while boundary conditions Eqs. (6b,c) are simply replaced by their approximations

$$\sigma^{bx}_{r\,1} = 0, \tag{19a,b}$$

$$\sigma^{bx}_{r\,K} = \frac{\sigma_0}{2}\,.$$

Eqs. (18)-(19a,b) can thus be written in the matrix form

$$\mathbf{A}\,\Sigma = \mathbf{m}, \tag{20}$$

where $\mathbf{A} \in \mathbb{R}^{K\times K}$ is a square tridiagonal matrix, $\mathbf{\Sigma} \in \mathbb{R}^K$ is a column vector whose elements are the variables $\sigma^{bx}_{r1}, \sigma^{bx}_{r2}, \cdots, \sigma^{bx}_{rk}$ and $\mathbf{m} \in \mathbb{R}^K$ is a column vector whose first $K-1$ elements are zeros and the last one is $\sigma_0/2$.

The same considerations can be taken into account for Eqs. (11)-(12a-d). Eq. (11) can be rewritten as the following system of $K-4$ algebraic equations

$$\begin{aligned} &g_{k+2}\left(2+\Delta r\,\alpha^{ps}_k\right) + g_{k+1}\left(-8-2\Delta r\,\alpha^{ps}_k + 2\Delta r^2\,\beta^{ps}_k + \Delta r^3\,\gamma^{ps}_k\right) + g_k\left(12 - 4\Delta r^2\,\beta^{ps}_k + 2\Delta r^4\,\delta^{ps}_k\right) \\ &+g_{k-1}\left(-8+2\Delta r\,\alpha^{ps}_k + 2\Delta r^2\,\beta^{ps}_k - \Delta r^3\,\gamma^{ps}_k\right) + g_{k-2}\left(2-\Delta r\,\alpha^{ps}_k\right) = 0 \end{aligned} \tag{21}$$

with k=3,4,…,K−2. Also here, the terms α^{ps}_k, β^{ps}_k, γ^{ps}_k and δ^{ps}_k can be derived by using the derivative approximations in Table 1 of their expressions. Finally, boundary conditions Eqs. (12a-d), with the aid of Eqs. (10a-c), can be approximated as follows

$$\frac{1}{a}\frac{g_3 + 4g_2 - 3g_1}{2\Delta r} - \frac{4g_1}{a^2} = 0, \tag{22a-d}$$

$$\frac{1}{a}\frac{g_3 + 4g_2 - 3g_1}{2\Delta r} - \frac{g_1}{a^2} = 0,$$

$$\frac{1}{A}\frac{g_{K-2} - 4g_{K-1} + 3g_K}{2\Delta r} - \frac{4g_K}{A^2} = \frac{\sigma_0}{2},$$

$$\frac{1}{A}\frac{g_{K-2} - 4g_{K-1} + 3g_K}{2\Delta r} - \frac{4g_K}{A^2} = -\frac{\sigma_0}{4},$$

respectively, where the far-field boundary conditions have been evaluated at the last discretization point $r_K = A \gg a = r_1$. The resulting system of equations can be recast in the matrix form

$$\mathbf{B}\,\Gamma = \mathbf{n}, \tag{23}$$

where $\mathbf{B} \in \mathbb{R}^{K\times K}$ is the a square pentadiagonal matrix, $\mathbf{\Gamma} \in \mathbb{R}^K$ is a column vector whose elements are the variables g_1,g_2,…, g_K and $\mathbf{n} \in \mathbb{R}^K$ is a column vector whose first $K-2$ elements are zeros and the last two are $\sigma_0/2$ and $-\sigma_0/4$, respectively. Elastic uniform biaxial and pure shear stresses are embedded into Eqs. (20) and (23), respectively, whose solutions are given by

$$\Sigma = \mathrm{inv}(\mathbf{A})\,\mathbf{m}, \tag{24}$$

and

$$\Gamma = \mathrm{inv}(\mathbf{B})\,\mathbf{n}\,. \tag{25}$$

where inv(·) is the inverse operator for square matrices.

The finite difference method has been implemented successfully for the computation of stresses arising in functionally graded bodies in several circumstances, e.g., [46-53]. Nevertheless, before proceeding

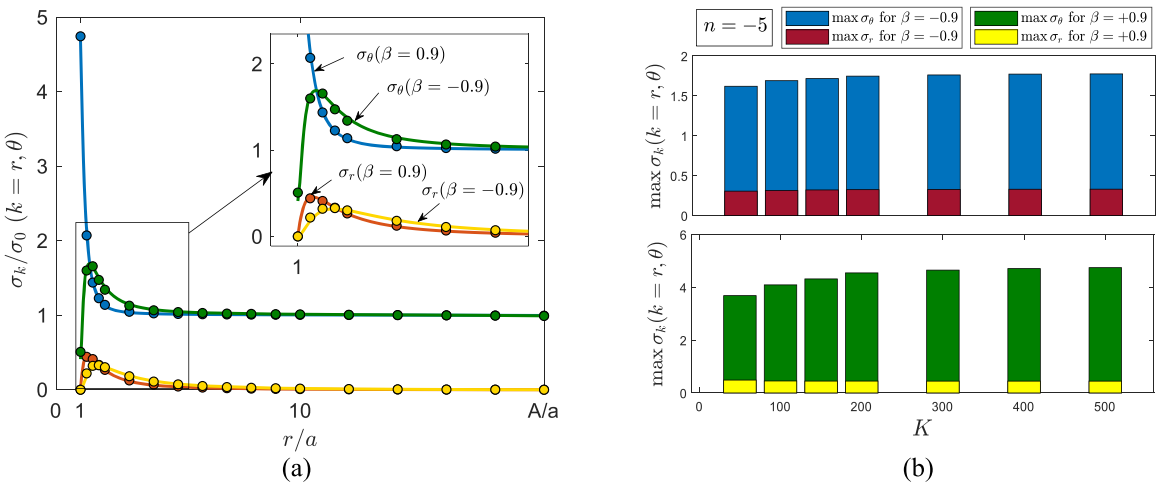

Fig. 5. (a) Analytical (solid lines) versus numerical (scatter points) solutions for the normalized radial and hoop stresses along the vertical line MN associated with the Young's modulus distribution in Eq. (14) with β = ±0.9 and $n = -5$. The parameters adopted for the simulation are $\nu = 0.3$ and $A/a = 20$. (b) Convergence study for the maximum radial and hoop stresses as functions of K.

with the solution of the optimization problem, an example showing the validation of the method is necessary. Analytical solutions for the stresses are thus borrowed from the literature and compared to the numerical results. Among others, closed-form solutions derived in [15] are taken into account, where mechanical properties are described by the general power-law (14) for β = ±0.9 and $n = -5$. Fig. 5a shows the analytical solutions for the radial and hoop stresses (solid lines) in the plate along MN and the numerical solutions (scatter points) by means of the finite difference method. A mesh convergence study has been carried out for the Young's modulus variation (14) adopted in [15] with β = ±0.9 and $n = -5$. In particular, it was found that the maximum values of the occurring stresses satisfy the convergence criterion $\sigma_{j,\max}^{(K_{i+1})} - \sigma_{j,\max}^{(K_i)} \leq 10^{-2}$MPa beyond $K = 300$, being i and $i+1$ two numerical forecasts employing K_i and K_{i+1} nodes, respectively, and $j = r, \theta$ (see Fig. 5b). Thus, the use of uniform grid was sufficient to accurately reproduce the stress field at the rim of the hole and without the need to adopt a finite difference discretization technique with non-uniform nodes. In fact, the use of finite difference schemes with a denser grid discretization near the hole will not lead to linear systems of algebraic equations for the unknown variables, like Eqs. (20) and (23), and therefore iterative techniques requiring one to resort to iterative techniques [54].

Eventually, the maximum operator appearing in Eq. (17) is replaced by its p-norm approximation (where p is an even number greater than or equal 2), given by

$$\sigma_{\theta,\max} \approx \left(\int_a^A \widehat{\sigma}_\theta(r)^p dr \right)^{\frac{1}{p}} \tag{26}$$

and evaluated by means of the well-known trapezoidal rule, namely

$$\widehat{\sigma}_{\theta,\max} \approx \left[\Delta r \left(\widehat{\sigma}_\theta(a)^p + \widehat{\sigma}_\theta(A)^p + \sum_{i=2}^{K-1} \widehat{\sigma}_\theta(r_i)^p \right) \right]^{\frac{1}{p}}. \tag{27}$$

Thus, Problem 1 can be transcribed into the following NLP problem (see the right part of the flowchart in Fig. 4).

Problem 2.	min	$\widehat{\sigma}_{\theta,\max} \approx \left[\Delta r\left(\widehat{\sigma}_{\theta\,1}^p + \widehat{\sigma}_{\theta\,K}^p + \sum_{i=2}^{K-1} \widehat{\sigma}_{\theta\,i}^p\right)\right]^{\frac{1}{p}}$
	$\mathbf{V} \in \mathbb{R}^K$	
	s.t.	$E_j = \widetilde{E}_1(1-V_j) + \widetilde{E}_2 V_j,\ j = 1, 2, \ldots, K$
		$\sum_{i=1}^K A_{ji}\,\sigma_{r\,i}^{bx} - m_j = 0,\ j = 1, 2, \ldots, K$
		$\sum_{i=1}^K B_{ji}\,g_i - n_j = 0,\ j = 1, 2, \ldots, K$
		$\widehat{\sigma}_{\theta\,j} = \sigma_{r\,j}^{bx} - r_j \frac{\sigma_{r\,j+1}^{bx} - \sigma_{r\,j-1}^{bx}}{2\Delta r} + \frac{g_{j+1} - 2g_j + g_{j-1}}{\Delta r^2},\ j = 2,3, \ldots, K-1$
		$\widehat{\sigma}_{\theta\,1} = \sigma_{r\,1}^{bx} - a\frac{-3\sigma_{r\,1}^{bx} + 4\sigma_{r\,2}^{bx} - \sigma_{r\,3}^{bx}}{2\Delta r} + \frac{2g_1 - 5g_2 + 4g_3 - g_4}{\Delta r^2},$
		$\widehat{\sigma}_{\theta\,K} = \sigma_{r\,K}^{bx} - A\frac{\sigma_{r\,K-2}^{bx} - 4\sigma_{r\,K-1}^{bx} + 3\sigma_{r\,K}^{bx}}{2\Delta r} + \frac{-g_{K-3} + 4g_{K-2} - 5g_{K-1} + 2g_K}{\Delta r^2},$

where the volume fraction has been replaced by a finite-dimensional vector $V = (V_1, V_2, \cdots, V_k) \in \mathbb{R}^K$, linked to Young's modulus through Eq. (1), being fixed the stiffness ratio $\widetilde{E}_2/\widetilde{E}_1$ and the exponent p for the objective function evaluation. The vector of the decision variables of the NLP problem consists of the K discrete variables V_1,V_2,…, V_K. The constraints are the discrete equations for the elastic problems Eqs. (6a-c) and (11)-(12a-d). The optimal solution therefore yields the optimal variation of the volume fraction and the corresponding stress behavior throughout the plate.

5. Results and discussion

In this Section, numerical optimal solutions for Problem 2 are illustrated and discussed. Hereinafter, the exponent p was taken to be equal to 200 (higher values generally lead to results too large to represent as conventional floating-point values during the iteration process), which yields a good approximation of the maximum hoop stress associated with the optimal solution, as confirmed by numerical results below. A gradient-based solver has been employed to numerically compute the optimal decision variable such that the maximum hoop stress reaches its minimum value. The algorithm used in this study is the well-known

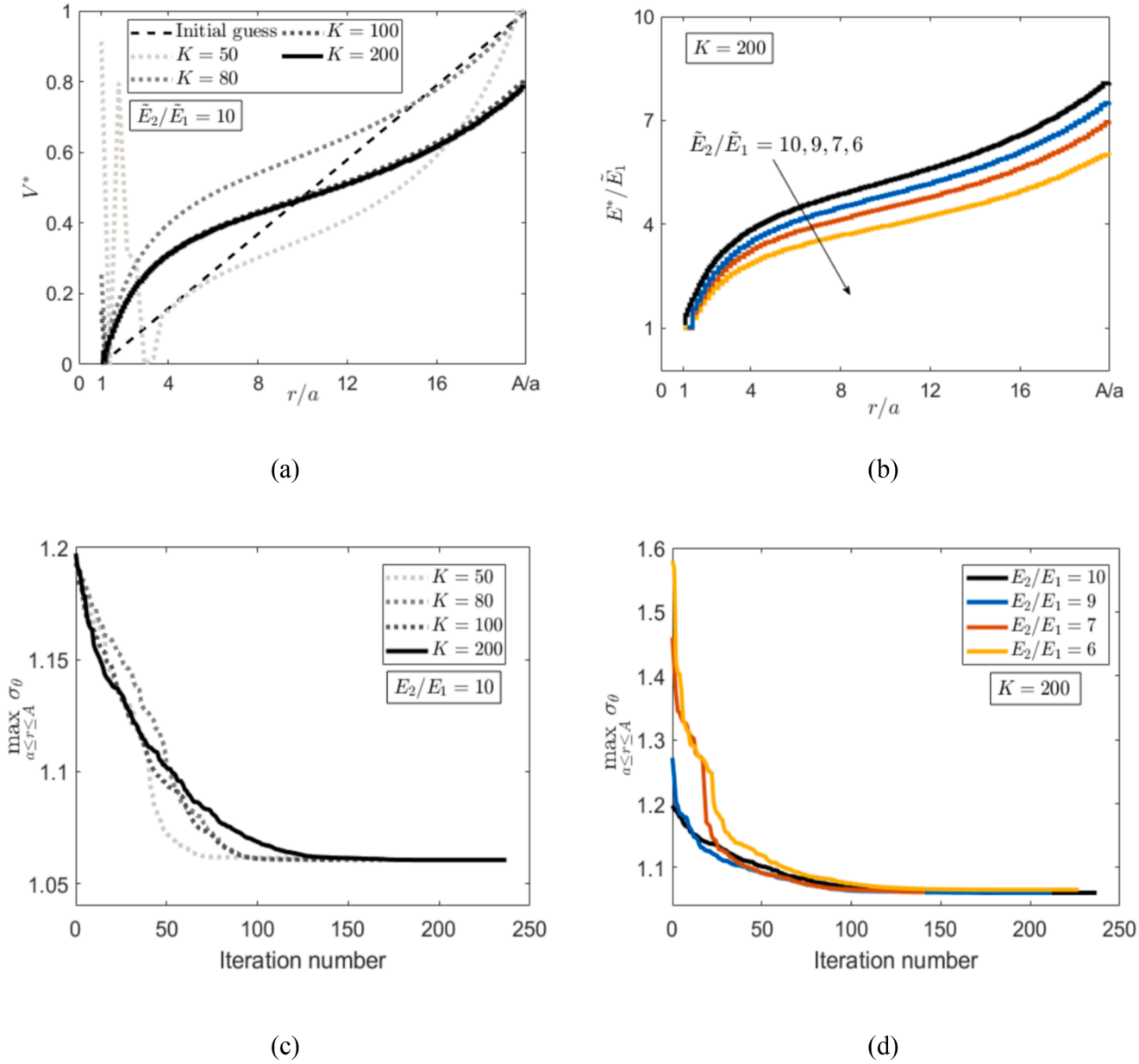

Fig. 6. (a) The linear initial guess (dashed line) as well as optimal numerical solutions (dotted and solid lines) for the volume fraction as K increases considering $E_2/E_1 = 10$. (b) Optimal solutions for the Young's modulus distribution considering different stiffness ratios. Numerical forecasts have been performed with $p = 200$ and $A/a = 20$. The history of the iterations is also reported in (c) and (d).

sequential quadratic programming algorithm [55]. Termination tolerances on both the function value as well as on the first-order condition for optimality have been imposed as 10^{-6}. In the light of conclusions made in [56], a linear volume fraction has been chosen as an initial guess and the numerical optimal solution has been sought iteratively.

For the sake of comparison with the result obtained in [15], a first simulation has been performed with a stiffness ratio $\widetilde{E}_2/\widetilde{E}_1 = 10$. The initial target is therefore to compare numerical results with the stress performance associated with the Young's modulus distribution obtained with $\beta = -0.9$ and $n = -5$ (see Figs. 2a,b or 5). Fig. 6a shows the initial guess (dashed line) and numerical optimal volume fractions with the same load and geometrical parameters as those employed for the validation example. More precisely, successive numerical solutions were obtained for increasing K values (dotted lines) until a prefixed convergence criterion between consecutive optimal solutions is achieved. In particular, the considered optimal solution ($K = 200$, solid line) was chosen instead of another ones associated with lower nodes (e.g., $K = 100$) as the norm of their difference is less than 10^{-2}. It is worth noting that the optimal volume fraction increases throughout the radial direction, indicating the optimality of adopting a softer material at the rim of the circular hole. This finding is in agreement with the literature reporting enhancement studies for the SCF for plates with circular holes (see, e.g., [10]). The resulting optimal Young's modulus distribution is following a sort of sigmoid function around the linear distribution. Moreover, the optimal material distribution does not necessarily assume, as base materials, the functionally graded material constituents at the boundaries of the plate. Similar forecasts have been performed for different stiffness ratios $\widetilde{E}_2/\widetilde{E}_1$, leading to the same conclusion (see Fig. 6b). For completeness, the history of iterations is reported in Figs. 6c,d.

To assess the stress performance of the optimal solution, the associated elastic hoop, radial and shear stresses are respectively illustrated in

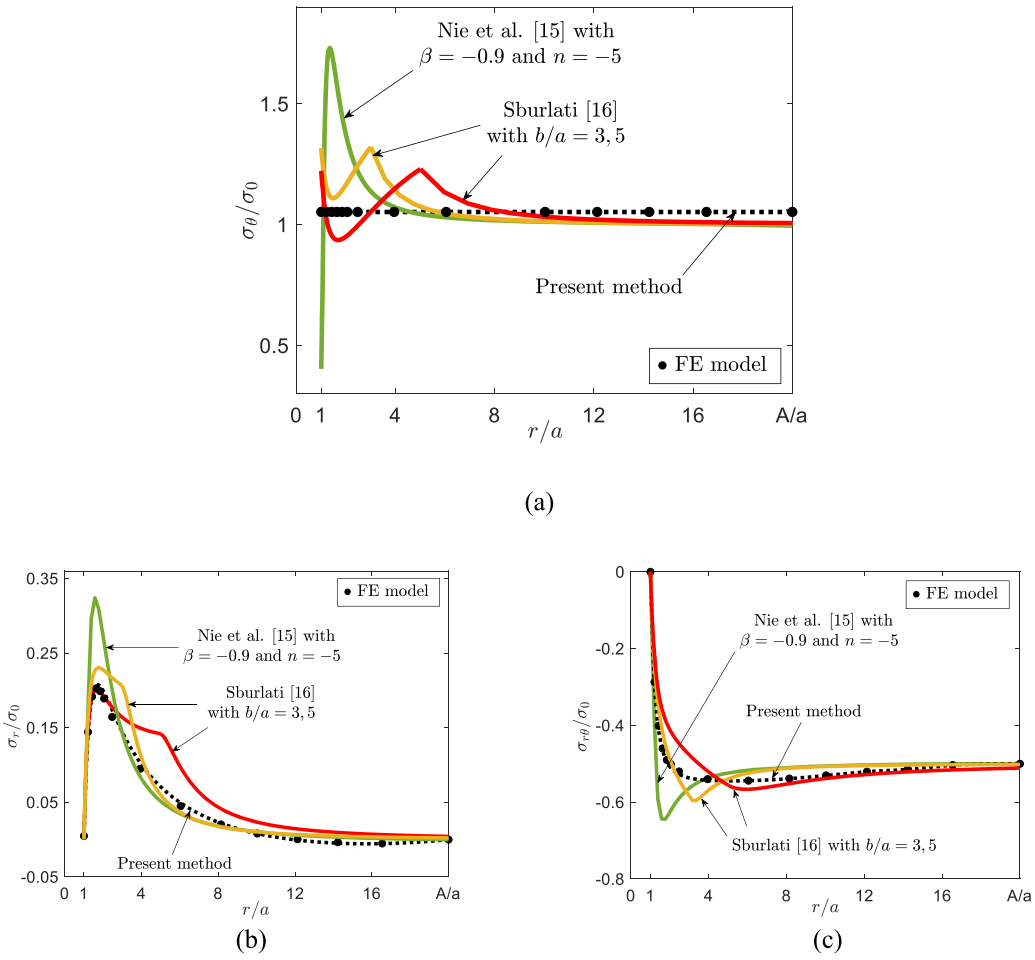

Fig. 7. Stresses associated with the optimal numerical solution (dotted lines) and finite element results (scatter points). (a) Hoop and (b) radial stresses along the vertical line MN and the (c) shear stress along $\theta = \pi/4$. Comparison between optimized stresses with results in literature (solid lines) [15,16].

Figs. 7a,b,c (dotted lines). It is worth appreciating that the hoop stress is uniform throughout the plate and free of stress peaks, yielding a plateaued stress behavior and thus making the stress concentration vanish throughout the radial domain. Moreover, the radial and shear stresses obey the boundary conditions of the problem. It is worth noting that the optimization output is the same if the uniaxial load direction is rotated by $\pi/2$, provided that the optimization problem is formulated on the line associated with $\theta = 0$. To further assess the correctness of the stress field obtained by the optimal Young's modulus distribution, a finite element (FE) forecast was carried out by commercial software. Due to symmetrical load and geometrical considerations, the geometrical domain consists of the quarter of the plate and is discretized by means of second-order quadrilateral plane stress elements. Necessary symmetric boundary conditions and the uniaxial load have been suitably applied to the model. The radial direction has been discretized into 200 radial strips (the same discretization points used in the transcription procedure), each of which is isotropic and homogeneous and has the same mechanical properties. Adjacent layers present different properties such that the resulting piecewise constant variation approximates the optimal Young's modulus distribution displayed in Fig. 6b. The FE stress behavior has been represented by scatter points, showing a remarkable fit with the optimization solver outputs, compared to the material modeling simplifications necessary for the FE forecast, and confirming the uniformity of the hoop stress on the line MN. Furthermore, a comparison between stresses obtained by the present approach alongside with those analytically derived in [15] (associated with $\beta = -0.9$ and $n = -5$) and in [16] for two different ring geometries ($b/a = 3$ and 5) is made (see solid lines). It is clear that the present approach leads to Young's modulus distributions (sigmoid-like curves) associated with the most uniform hoop stress (and consequently the minimum peak hoop stress) throughout the plate.

6. Conclusions

The optimization of the volume fraction distribution to minimize peak hoop stresses in functionally graded infinite plates with a circular hole and subjected to uniaxial traction is numerically addressed. The optimization problem has been stated and formulated as a dynamic optimization problem, where the variation of the decision variable, namely the volume fraction and consequently the Young's modulus through the rule of mixture, is unknown beforehand and not limited to specified functions along the radial direction. The problem has been divided into two sub-problems, i.e., occurring stresses have been assumed as the superposition of those resulting from the biaxial and from the pure shear deformations. Optimality conditions for the best distribution of the volume fraction could not be solved analytically, hence numerical methods were necessary.

The transcription procedure consisted in approximating the peak stress by the trapezoidal rule and converting the differential equations accounting for the elastic problem into two systems of algebraic equations describing the two sub-problems by means of the finite difference method due to the simplicity of the employed boundary conditions which permitted the solution with reduced computational costs. The obtained numerical solutions for the Young's modulus follow a sigmoidal behavior. The associated hoop stress revealed uniform along the radius and has been validated by the finite element method.

The Young's modulus distribution has been assumed to follow the rule of mixture; however, other models for the effective Young's modulus can be fitted in the same framework. The present article can be considered as a preliminary study whose results can be further extended to other geometrical discontinuities or to plates of finite dimensions, provided that the finite difference method is replaced by the finite element method. In fact, other noncircular holes such as elliptic, rectangular slots with rounded edges or rounded-square cutouts require the use of numerical methods capable of transcribing the governing elasticity equations not anymore in a 1D geometrical domain as in the case of plates with a circular hole (along MN), but along the whole 2D geometrical domain. From the technological point of view, the availability of advanced fabrication routes, e.g. additive manufacturing and spark plasma sintering, has been making the fabrication of these materials with tailored morphologies and structural properties possible, as stated in [57].

Funding

Funded by the European Union NextGenerationEU.

CRediT authorship contribution statement

Hassan Mohamed Abdelalim Abdalla: Writing – original draft, Validation, Software, Methodology, Formal analysis, Conceptualization. **Francesco De Bona:** Writing – review & editing, Supervision, Methodology, Conceptualization. **Daniele Casagrande:** Writing – review & editing, Validation, Supervision, Investigation, Formal analysis.

Declaration of competing interest

The authors declare that they have no known competing financial interests or personal relationships that could have appeared to influence the work reported in this paper.

Data availability

No data was used for the research described in the article.

References

[1] E.G. Kirsch, Die Theorie der Elastizität und die Bedürfnisse der Festigkeitslehre, Zeitschrift des Vereines deutscher Ingenieure 42 (1898) 797–807.
[2] R.D.B. Sevenois, S. Koussios, Analytic methods for stress analysis of two-dimensional flat anisotropic plates with notches: an overview, Appl. Mech. Rev. 66 (6) (2014) 060802.
[3] S. Anoop Kumar, R. Rajesh, S. Pugazhendhi, A review of stress concentration studies on fibre composite panels with holes/cutouts, in: Proceedings of the Institution of Mechanical Engineers, Part L: Journal of Materials: Design and Applications 234, 2020, pp. 1461–1472.
[4] B.G. Korenev, Punch lying on as elastic half-space whose modulus of elasticity is a function of the depth, Dokl. Akad. Nauk. 112 (1957) 823–826.
[5] G.I. Popov, Bending of an unbounded plate supported by an elastic half-space with a modulus of elasticity varying with depth, J. Appl. Math. Mech.s 23 (6) (1959) 1566–1573.
[6] R.E. Gibson, Some results concerning displacements and stresses in a non-homogeneous elastic half-space, Geotechnique 17 (1) (1967) 58–67.
[7] C.O. Horgan, A.M. Chan, The pressurized hollow cylinder or disk problem for functionally graded isotropic linearly elastic materials, J. Elast 55 (1999) 43–59.
[8] J.F. Durodola, O. Attia, Deformation and stresses in functionally graded rotating disks, Compos. Sci. Technol. 60 (2000) 987–995.
[9] T. Singh, V.K. Gupta, Effect of anisotropy on steady state creep in functionally graded cylinder, Compos. Struct. 93 (2011) 747–758.
[10] D.V. Kubair, B. Bhanu-Chandar, Stress concentration factor due to a circular hole in functionally graded panels under uniaxial tension, Int. J. Mech. Sci. 50 (2008) 732–742.
[11] T.A. Enab, Stress concentration analysis in functionally graded plates with elliptic holes under biaxial loadings, Ain Shams Eng. 5 (2014) 839–850.
[12] M. Mohammadi, J.R. Dryden, L. Jiang, Stress concentration around a hole in a radially inhomogeneous plate, Int. J. Solids. Struct. 48 (2011) 483–491.
[13] Q. Yang, C.F. Gao, W. Chen, Stress analysis of a functional graded material plate with a circular hole, Arch. Appl. Mech. 55 (7) (2010) 1263–1271.
[14] M. Kushwaha, P.K. Saini, An analytical approach to reduce the stress concentration around a circular hole in a functionally graded material plate under axial load, Appl. Mech. Mater. 592-594 (2014) 985–989.
[15] G.J. Nie, Z. Zhong, R.C. Batra, Material tailoring for reducing stress concentration factor at a circular hole in a functionally graded material (FGM) panel, Compos. Struct. 205 (2018) 49–57.
[16] R. Sburlati, Stress concentration factor due to a functionally graded ring around a hole in an isotropic plate, Int. J. Solids. Struct. 50 (2013) 3649–3658.
[17] R. Sburlati, S.R. Atashipour, S.A. Atashipour, Reduction of the stress concentration factor in a homogeneous panel with hole by using a functionally graded layer, Composite 61 (2014) 99–109.
[18] S. Nikbakht, S. Kamarian, M. Shakeri, A review on optimization of composite structures Part II: functionally graded materials, Compos. Struct. 214 (2019) 83–102.
[19] P. Nayak, A. Armani, Optimal design of functionally graded parts, Metals. 12 (8) (2022) 1335.
[20] A. Ghazanfari, M.C. Leu. Composition optimization for functionally gradient parts considering manufacturing constraints. In: *Proceedings of the ASME 2014 international manufacturing science and engineering conference collocated with the JSME 2014 international conference on materials and processing and the 42nd north american manufacturing research conference*, Detroit, MI, USA, 9–13 June 2014.
[21] M. Jamshidi, J. Arghavani, Optimal design of two-dimensional porosity distribution in shear deformable functionally graded porous beams for stability analysis, Thin-Walled Struct. 120 (2017) 81–90.
[22] H.M. Abo-Bakr, R.M. Abo-Bakr, S.A. Mohamed, M.A. Eltaher, Weight optimization of axially functionally graded microbeams under buckling and vibration behaviors, Mech. Based Design Struct. Mach. 51 (1) (2020) 213–234.
[23] A.W. Leissa, M. Vagins, The design of orthotropic materials for stress optimization, Int. J. Solids. Struct. 14 (1978) 517–526.
[24] K. Tian, X. Ma, Z. Li, S. Lin, B. Wang, A.M. Waas, A multi-fidelity competitive sampling method for surrogate-based stacking sequence optimization of composite shells with multiple cutouts, Int. J. Solids. Struct. 193-194 (2020) 1–12.
[25] A. Nouri, S. Astaraki, Optimization of sound transmission loss through a thin functionally graded material cylindrical shell, Shock Vibrat. (2014) 814682.
[26] H.M.A. Abdalla, D. Casagrande, L. Moro, Thermo-mechanical analysis and optimization of functionally graded rotating disks, J. Strain Analy. Eng. Des. 55 (5–6) (2020) 159–171.
[27] A.M. Eldeeb, Y.M. Shabana, A. Elsawaf, Particle swarm optimization for the thermoelastic behaviors of functionally graded rotating nonuniform thickness sandwich discs, Arab. J. Sci. Eng. 48 (2022) 4067–4079.
[28] R. Madan, S. Bhowmick, Optimum FG rotating disk of constant mass: lightweight and economical alternatives based on limit angular speed, Iranian J. Sci. Techn. 47 (3) (2023) 1019–1033. *Transactions of Mechanical Engineering*.
[29] Z.W. Wang, Q. Zhang, L.Z. Xia, J.T. Wu, P.Q. Liu, Stress analysis and parameter optimization of an FGM pressure vessel subjected to thermo-mechanical loadings, Procedia Eng. 130 (2015) 374–389.
[30] Z.W. Wang, Q. Zhang, L.Z. Xia, J.T. Wu, P.Q. Liu, Thermomechanical analysis of pressure vessels with functionally graded material coating, J. Press. Vessel. Technol. 138 (1) (2016) 011205.
[31] M. Khorsand, Y. Tang, Thermal analysis and electro-elastic response of multilayered spherical vessels, Internat. J. Pressure Vessels Pip. 171 (2019) 194–206.
[32] R. Chiba, Y. Sugano, Optimisation of material composition of functionally graded materials based on multiscale thermoelastic analysis, Acta Mech. 223 (2012) 891–909.
[33] Q.X. Lieu, J. Lee, Modeling and optimization of functionally graded plates under thermo-mechanical load using isogeometric analysis and adaptive hybrid evolutionary firefly algorithm, Compos. Struct. 179 (2017) 89–106.
[34] F. Moleiro, J. Madeira, E. Carrera, J.N. Reddy, Design optimization of functionally graded plates under thermo-mechanical loadings to minimize stress, deformation and mass, Compos. Struct. 245 (2020) 112360.
[35] R.C. Batra, Material tailoring and universal relations for axisymmetric deformations of functionally graded rubberlike cylinders and spheres, Math. Mech. Solids 16 (7) (2011) 729–738.
[36] J. Nie, Z. Zhong, R.C. Batra, Material tailoring for functionally graded hollow cylinders and spheres, Composite Sci. Techn. 71 (2011) 666–673.
[37] M. Carraturo, E. Rocca, E. Bonetti, D. Homberg, A. Reali, F. Auricchio, Graded-material design based on phase-field and topology optimization, Comput. Mech. 64 (2019) 1589–1600.
[38] T. Hu, Y. Wang, H. Zhang, H. Li, X. Ding, K. Izui, S. Nishiwki, Topology optimization of coated structures with layer-wise graded lattice infill for maximizing the fundamental eigenfrequency, Comput. Struct. 271 (2022) 106861.
[39] H.M.A. Abdalla, D. Casagrande, F. De Bona, A dynamic programming setting for functionally graded thick-walled cylinders, Materials. (Basel) 13 (2020) 3988.
[40] H.M.A. Abdalla, D. Casagrande, An intrinsic material tailoring approach for functionally graded axisymmetric hollow bodies under plane elasticity, J Elast 144 (2021) 15–32.
[41] H.M.A. Abdalla, D. Boussaa, R. Sburlati, D. Casagrande, On the best volume fraction distributions for functionally graded cylinders, spheres and disks – A pseudospectral approach, Compos. Struct. 311 (2023) 116784.
[42] Y. Zhou, Q. Lin, J. Hong, N. Yang, Optimal design of functionally graded material for stress concentration reduction, Structures 29 (2021) 561–569.
[43] Y. Miyamoto, W.A. Kaysser, B.H. Rabin, A. Kawasaki, R.G. Ford, Function. Graded Mater.. Design, Process. Appl.. (1999).
[44] S.P. Timoshenko, J.N. Goodier, Theory of Elasticity, McGraw Hill Higher Education, New York, 1970.

[45] J. Stoer, R. Burlisch, Introduction to numerical analysis, Springer-Verlag, New York, 1980.
[46] Y. Zheng, H. Bahaloo, D. Mousanezhad, E. Mahdi, A. Vaziri, H. Nayeb-Hashemi, Stress analysis in functionally graded rotating disks with non-uniform thickness and variable angular velocity, Int. J. Mech. Sci. 119 (2016) 283–293.
[47] A.M. Eldeeb, Y.M. Shabana, A. Elsawaf, Influences of angular deceleration on the thermoelastoplastic behaviors of nonuniform thickness multilayer FGM discs, Compos. Struct. 258 (2021) 113092.
[48] B.L. Wang, Z.H. Tian, Application of finite element–finite difference method to the determination of transient temperature field in functionally graded materials, Finite Ele. Analy. Design 41 (4) (2005) 335–349.
[49] A. Dorogoy, Finite difference method for solving crack problems in a functionally graded material, Simulation. 95 (10) (2018) 941–953.
[50] P.R. Sarkar, A.S. Rahman, Finite-difference analysis of stresses of a non-uniform functionally graded material circular disk rotating in the magneto-thermal environment: an equal mass study, J. Mater. 237 (2) (2023) 301–316.
[51] P. Das, M.A. Islam, S. Somadder, M.A. Hasib, Analytical and numerical analysis of functionally graded (FGM) axisymmetric cylinders under thermo-mechanical loadings, Mater. Today Commun. 33 (2022) 104405.
[52] M. Dorduncu, M.K. Apalak, Stress wave propagation in adhesively bonded functionally graded circular cylinders, J. Adhes. Sci. Technol. 30 (12) (2016) 1281–1309.
[53] M. Dorduncu, M.K. Apalak, J.N. Reddy, Stress wave propagation in a through-thickness functionally graded adhesive layer, J. Adhes. Sci. Technol. 33 (21) (2019) 2329–2355.
[54] D. Xu, X. Deng, Y. Chen, G. Wang, Y. Dong, Effect of nonuniform grids on high-order finite difference method, Adv. Appl. Math. Mech. 9 (4) (2017) 1012–1034.
[55] S.S. Rao, Optimization: theory and applications, Wiley Eastern Ltd, New Delhi, 1978.
[56] H.M.A. Abdalla, D. Casagrande, F. De Bona, Analysis of stress concentration in functionally graded plates with linearly increasing young's modulus, Materials. 16 (2023) 6882.
[57] M. Naebe, K. Shirvanimoghaddam, Functionally graded materials: a review of fabrication and properties, Appl. Mater. Today 5 (2016) 223–245.